# Supplementary Materials for

## Transcription-coupled changes in nuclear mobility of mammalian cis-regulatory elements

Bo Gu, Tomek Swigut, Andrew Spencley, Matthew R. Bauer, Mingyu Chung, Tobias Meyer, Joanna Wysocka*

*Corresponding author. Email: wysocka@stanford.edu

Published 25 January 2018 on *Science* First Release
DOI: 10.1126/science.aao3136

**This PDF file includes:**



**Other Supplementary Material for this manuscript includes the following:**
(available at www.sciencemag.org/cgi/content/full/science.aao3136/DC1)

## Materials and Methods

DNA constructs

PB-TRE3G-dCas9-eGFP-WPRE-ubcp-rtta-IRES-puroR was generated by cloning dCas9-eGFP into custom piggybac vector (hereafter referred to as PB-TRE3G) modified from the basic piggybac transposon backbone PB51x Dual Promoter Series (System Biosciences cat # PB510B-1). PB-TRE3G is a dual promoter backbone with TRE3G (Tet-on) promoter followed by ubiquitin C promoter (ubqc). Reverse tetracycline-controlled transactivator (rtta) is driven by ubqc promoter and is followed by IRES-puromycin resistance cassette. dCas9-eGFP was PCR amplified from published construct obtained from Addgene (plasmid # 51023) and was assembled into PB-TRE3G digested with AgeI and XbaI through Gibson assembly downstream of TRE3G promoter.

pGEMT-hU6-spSL for CARGO assembly was generated through Gibson assembly of hU6 and modified S. pyogenes scaffold sequence (11) into pGEMT backbone (Promega). px332/px333 for CARGO assembly were modified from pX330-U6-Chimeric_BB-CBh-hSpCas9 obtained from Addgene (plasmid # 42230) by mutating all BpiI sites and replacing spCas9 with mcherry/tagBFP (with BpiI synonymous mutations in the ORFs).

Stable dCas9-eGFP mESC Cell line generation

Early passage mESCs were transfected with PB-TRE3G-dCas9-eGFP-WPRE-ubcp-rtta-IRES-puroR construct along with super piggybac transposase plasmid PB210PA-1 (Systems Biosciences cat # PB210PA-1) in a 1:1 (mass) ratio using lipofectamine 2000 (thermofisher scientific). 48 hrs after dCas9-eGFP construct transfection, cells were subject to puromycin selection for 7 days. On day 8, doxycycline (Dox) was added to the puromycin resistant cells for 24 hrs followed by FACS sorting of single cells with low GFP level into single wells of 96-well plate. Single cells were then expanded for 10 days and then transferred to glass-bottom 96-well plate for microscopy-assisted screening of cell lines with proper Dox-induced dCas9-eGFP expression level. Furthermore, as a second pass for microscopy-assisted screening, guide RNA targeting telomeric repeats were transfected 24 hrs prior to live-cell imaging. Cell lines with higher signal-to-background ratio of telomeric puncta were chosen as candidates for CARGO labeling.

Cell culture and differentiation

Male mouse ESC lines (R1) were grown in serum-free N2B27-based medium supplemented with MEK inhibitor PD0325901 (0.8 μM) and GSK3β inhibitor CHIR99021 (3.3 μM) in tissue culture (TC) dishes pretreated with 7.5 μg/ml polyL-ornithine (Sigma) and 5 μg/ml laminine (BD) (*17*).

To induce EpiLC differentiation, cells were washed with PBS, trypsinized, and strained. Cells were plated at a seeding density of $2\times10^4$ cells/cm$^2$ on TC dishes pretreated with 10 μg/ml Fibronectin (Millipore) in AFK medium: N2B27-based medium supplemented with 1% KSR (Invitrogen) and 12 μg/ml bFGF (Peprotech).

CARGO array assembly

CARGO assembly relies on two basic building blocks, including constant region, which consist of modified S. pyogenes scaffold sequence (fusion sequence of S. pyogenes crRNA and tracrRNA) (*11*), followed by RNA polIII terminator, followed by human U6 promoter; and

synthetic variable regions, which are composed of second half of the preceding guide RNA followed by first half of the following guide RNA separated by a spacer composed of two inverted with respect to each other BpiI sites.

The protocol consists of 1). constant region preparation and 2). array assembly.

In the constant region preparation step, constant region with proper sticky ends is released by digesting pGEMT-hU6-spSL (custom generated) plasmid with BsmBI. The released constant region is separated from the pGEMT backbone on 1% agarose gel and gel purified with commercial kit (Macherey-Nagel).

Oligonucleotides (50-60 bp) with variable regions were ordered through IDT. Upon receiving, forward and reverse oligos are annealed and phosphorylated and stored at -20°C.

In the array assembly step, annealed chimeric oligo is mixed with digested constant region, and a minimum of 4-hr ligation with high-concentration T4 ligase (Thermofisher Scientific) was performed. The ligation step yields ligation products (hereafter referred to as minicircles). Next, a stoichiometry check with 1% agarose gel is performed with 1/10 of the minicircles stained with sybr-gold (Thermofisher Scientific). After stoichiometry check, individual minicircles were treated with plasmid-safe exonuclease to clean up the un-ligated products. Then, plasmid-safe exonuclease treated individual minicircles were pooled together and column-purified (Zymo Research). The pooled circle mixes were assembled directly into the digested final destination vector px332/px333 through optimized golden gate assembly reaction (*27*). Next, 1/5 of golden gate reaction was inspected by agarose gel stained with sybr-gold to check for the expected assembly intermediate product. 4/5 of the golden-gate reaction was then subject to plasmid-safe exonuclease (Epicentre) treatment. exo-nuclease treated reaction was transformed into competent cells (Bioline). For each plate, individual colonies were picked for plasmid purification with miniprep kit (Macherey-Nagel) and test digestion with Acc65I, KpnI and XbaI. Plasmids with correct digestion pattern were then verified by Sanger sequencing and retransformed followed by nucleobond-extra midi/maxi kit (Macherey-Nagel).

In summary, the optimized method is straightforward (with a 3-day workflow), robust [with assembly efficiency of 100% for octamers, ~70% for dodecamer (12-mers) and ~60% for octadecamers (18-mers), fig. S1A, B], and accurate (as confirmed by Sanger sequencing of multiple clones).

For a detailed CARGO assembly bench protocol, see additional protocol.

Live-cell image acquisition of dCas9-CARGO imaging

Briefly, on day 0, low passage dCas9-eGFP mESC cell lines were plated into 24-well plate (Corning) at a seeding density of $2\times10^5$ cells/well with Dox to induce dCas9 expression. On Day 1, cells were transfected with 3×0.67 ug (total of 2ug) of CARGO arrays, each harboring 12 different guide RNAs. On day 2, 12 hrs post-transfection, cells were trypsinized and replated onto live-cell chamber. For imaging in mESC state, cells were imaged on the next day (day 3). For imaging coupled with differentiation, trypsinized cells were plated at a density of $1\times10^4$ cells/chamber of 4-well lab-tek chamber II (Thermofisher Scientific) coated with 10 ug/ml fibronectin (Millipore). Cells were grown either in 2i + Lif media or AFK media for 48 hrs with one round of media changing at 24 hrs before conducting live-cell imaging.

Live-cell dCas9 images and data shown in Figs 2-4 and Movies S1-5 were acquired using Nikon Eclipse Ti-E microscopy stand with a CSU-W1 (Yokogawa) confocal unit and an 60x Nikon PlanApo water-immersion objective of 1.27 NA, a motorized stage (ASI) enclosed by an environmental chamber, and an sCMOS camera (Andor Zyla 4.2). The excitation of GFP is

achieved by a 488 nm laser (100 mW). In the imaging and bin setting used for live-cell data acquisition, the effective pixel size is 108.3 nm×108.3 nm. Acquisition was controlled by slidebook software (Intelligent Imaging Innovations). All images were acquired at a frame rate of 5Hz for 500 frames with an exposure time of 100/150ms, and with the temperature maintained at 37 °C by live-cell chamber. For all time-series, either 256×256 pixels or 512×512 pixels cell-containing subframes were collected to minimize storage usage. Notably, to achieve better temporal resolution and minimize photobleaching as well as to get better statistical power for tMSD analysis, we performed live-cell imaging without going through z series of the whole nuclei. In the specific live-cell imaging scheme, we achieve minimal time interval of 200 ms/frame.

Live-cell dCas9 images shown in Fig 1D were acquired using a custom-built widefield-fluorescence system built around a Zeiss Axiovert 200M microscope, enclosed in an environmental chamber (Haison), outfitted with a CRISP autofocus system (Applied Scientific Instrumentation), an ORCA Flash 4.0 LT sCMOS camera (Hamamatsu, EPI light path) and a 100 W HBO lamp. A 63× 1.2 NA C-Apochromat water immersion objective was used and the system was controlled using μManager.

Additional notes on dCas9-CARGO live-cell labeling: we noticed that the labeling efficiency is highly sensitive to gRNA concentration and thus transfection efficiency. As transient transfection has been implemented in all the CARGO labeling and live-cell data acquisition in this study, we noticed a considerable variability of labeling efficiency between different rounds of experiments. We expect that imaging will be substantially improved by creation of stable CARGO-integrated cell lines.

Single-particle tracking and MSD analysis

For each time series, further image cropping was performed to facilitate local maxima identification. All the further-cropped image series were processed by a customized matlab script modified from IDL tracking package (http://www.physics.emory.edu/faculty/weeks//idl/). Briefly, for each time frame, pixel-precision local maxima was firstly segmented with a box filter. Local maxima at each time frame was further fitted by gaussian mask with least-squared fitting. The fitting process then estimated the local maxima position at sub-pixel-precision. Then trajectory connection was performed via finding nearest neighbors. Trajectories shorter than 50 time frames were discarded from downstream analysis. Time-averaged MSD (tMSD) analysis was performed with the position information retrieved from the single particle tracking of each trajectory through a customized matlab script following the equation:

$$MSD(n\Delta\tau) = \frac{1}{N-1-n}\sum_{i=1}^{N-1-n}\left[r\left(i\Delta\tau + n\Delta\tau\right) - r(i\Delta\tau)\right]^2$$

After MSD was calculated and plotted in log-log space, least absolute deviations (LAD) (https://www.mathworks.com/help/curvefit/least-squares-fitting.html), a method for robust linear squares fitting which minimizes the influence of outliers usually appear within shorter time regime in MSD analysis due to localization error (*28*), was performed for each trajectory to fit the general motion equation:

$$MSD(t) = 4D_{app}t^{\alpha}$$

The fitting procedure then yielded $\log(4D_{app})$ = MSD (t = 1s) and α = slope. Specifically, for scaling exponent α, in systems characterized by a typical diffusion, MSD is directly proportional to time and scaling is linear with α = 1. However, particles in crowded macromolecular systems have in some cases been shown to exhibit anomalous diffusive behavior

with $0 < \alpha < 1$. To avoid the potential confounding effect of gross cell movement and rotation, we calculated MSD within only the first decade of time from 200ms to 8s (spanning maximum 40 timeframes with data from all 500 frames), during which there is negligible cell movement. Calculated MSD values are then plotted over time intervals for individual trajectory, each representing movement of an individual enhancer allele in a single cell.

Time- and ensemble-averaged MSD (eMSD) were calculated by averaging MSD of each time point from individual trajectories for all tracked trajectories followed by a time averaging defined as follow:

$$eMSD = \frac{1}{n}\sum_{i=1}^{n}\frac{1}{m}\sum_{j=0}^{m}(x_j(r_i+t)-x_j r_i)^2$$

The velocity autocorrelation function, $C_v^{\delta}(\tau)$, is calculated as follow:

$$C_v^{\delta}(\tau) = \langle v(t+\tau)\cdot v(t)\rangle$$

$$v(\delta) = \frac{1}{\delta}(r(t+\delta)-r(t))$$

This function indicates to what degree the average velocity over a time interval $\delta$ is correlated with the average velocity over another time interval $\delta$ that is separated by $\tau$ from the first one (*19*). A negative value of $C_v^{\delta}(\tau)$ indicate negative correlations (reversal) in velocity of labeled loci caused by elastic component ("push back") of the viscoelastic response within the cellular environment.

Analysis of the locus mobility distribution across cell states

Given that the distribution of $D_{app}$ is known to be log-normal (*8*) , Gaussian-mixture models were fitted by expectation–maximization algorithm as implemented in flexmix package (R) (*29*). Optimal number of components to fit was chosen based on Bayesian Information Criterion (BIC) (*30*) extracted from the stepFlexmix object containing alternative fits from single to five-component. Differences in distribution between ESC and EpiLC condition was determined with Kolmogorov-Smirnov test (ks.test in R).

Chromatin-immunoprecipitation

ChIP assays were performed as previously described with slight modification (*31*, *32*). In brief, mESC cells were cross-linked with 1% formaldehyde for 10 min at room temperature and quenched with glycine to a final concentration of 0.125 M for another 10 min. Chromatin was sonicated with a Bioruptor (Diagenode), cleared by centrifugation, and incubated overnight at 4 °C with 5–7 μg of the desired antibodies: anti-GFP (life technology cat # A11122) and anti-H3K27ac (active motif cat # 39133). Immunocomplexes were immobilized with 100 μl of protein-G Dynal magnetic beads (Life Technologies) for 4 h at 4 °C, followed by stringent washes and elution. Eluates were reverse cross-linked overnight at 65 °C and deproteinated with proteinase K at 56 °C for 30 min. DNA was extracted with phenol chloroform, followed by ethanol precipitation. ChIP-qPCR analyses were performed in a Light Cycler 480II (Roche). ChIP-qPCR signals were calculated as percentage of input.

Sequential immunofluorescence DNA fluorescence in-situ hybridization

Immunofluorescence was performed as described before (*33*). Briefly, cells were fixed with 4% PFA for 10min at RT followed by permeabilization with 0.5% triton X-100 in PBS for 10 min on ice. Samples were then blocked with 1% BSA in 0.1% triton-x 100 in PBS (IF buffer) for 30min. Next, anti-GFP antibody (1:100, chicken pAb anti GFP, cat # ab13970) diluted in IF

buffer was applied to the sample for 1 hr at RT followed by 3× washes with IF buffer. Next, Alexa-488 conjugated secondary antibody (1:1000) diluted in IF buffer was applied to the sample and incubated at RT for 1hr followed by 3x thorough washes with IF buffer. A post-fixation procedure with 3% PFA was performed after the immunofluorescence for 10 min at RT. After post-fixation, a re-permeabilization step was performed with 0.1 M HCl in 0.7% triton-x 100 PBS for 10min on ice. Next, DNA FISH was performed as described (*33*). Briefly, coverslips were equilibrated in 20% glycerol in PBS for at least 1hr followed by 3× freeze-thaws in liquid nitrogen. Coverslips were pre-denatured in 2xSCC in 50% de-ionized formamide for at least 1hr. Next, probes and cells on coverslips were heat-denatured simultaneously on heat-block (time and temperature were optimized for each FISH probe individually). After heat-denaturation, cells were hybridized with DNA FISH probes at 42°C overnight. On day 2, coverslips were washed 3× with 2xSSC followed by DAPI counterstaining. The stained coverslips were then mounted and subject to microscopic observation.

Live-fix correlative imaging

live-cell imaging was performed and acquired as described above. For correlative imaging, positions of individual cells with labeled dCas9 puncta were recorded and a maximum of 20 cells were recorded before fixation (30 min maximum between the start of recording and fixation). Next, 2× of PBS washes were applied before fixation with 4% PFA at RT for 30 min. After fixation, smFISH were performed following the instruction from the smFISH kit (Affymetrix). Briefly, cells were permeabilized after fixation and 3 consecutive rounds of hybridization with different probes provided by the kit were performed with 3× washes in between consecutive rounds of hybridization. After final round of hybridization, 1× of extensive wash was performed followed by nucleus counterstaining with DAPI. For image acquisition of smFISH for matched cells, the recorded live-cell positions were retrieved after plate was equilibrated in 37°C chamber for 15min. images were acquired with the same Nikon Eclipse Ti-E scope with CSU-W1 confocal unit with 2×2 binning. In this imaging settings, the effective pixel size was 216.6 nm×216.6 nm. All images were acquired as 10 μm zstack with z-step of 0.5 μm and maximum projected images were used for downstream analysis.

PolII inhibition live-cell experiment

Briefly, on day 0, low passage dCas9-eGFP mESC cell lines were plated into 24-well plate (Corning) at a seeding density of $2\times10^5$ cells/well with Dox to induce dCas9 expression. On Day 1, cells were transfected with 3×0.67 ug (total of 2ug) of CARGO arrays, each harboring 12 different guide RNAs. On day 2, 12 hrs post-transfection, cells were trypsinized and replated into 96-well glass-bottom plate (thermofisher scientific). For *Fgf5* enhancer labeling experiment, cells were plated at a seeding density of $1\times10^4$ cells/well supplemented with AFK media to induce mEpiLC differentiation. For *Tbx3* promoter labeling experiment, cells were plated at the same seeding density supplemented with 2i + Lif media to maintain mESC state. On day 4, 48 hrs post-replating, for each well, positions of 10-15 Cells with positively labeled dCas9 puncta were recorded. After live-cell imaging acquisition of all the recorded cells, same volume of imaging media as the working volume for 96-well plate with 2x final concentration of PolII inhibitors were spiked into the well. Final concentration of DRB, flavopiridol and triptolide were 100 μM, 2.2 μM and 10 μM, respectively.

Based on the estimation from the documented PolII traveling speed (~3 kb/min) (*34*) and *Fgf5/Tbx3* gene length (22kb/14kb), it will take on average ~10min for PolII to complete one

round of transcription at the gene bodies. Thus, with the purpose of inhibiting traveling PolII on either gene bodies before one round of transcription, image acquisition of the drug-treated cells started at 10, 15 and 10 min post spike-in for DRB, flavopiridol and triptolide, respectively. Cells with the recorded positions were re-visited and the live-cell acquisition was performed in the same manner as as pre-drug treatment. The above procedure was repeated for multiple wells within the same 96-well plate consecutively. All images were taken at a frame rate of 5Hz for 300 frames.

Single-molecule RNA FISH analysis

Cell nuclei were segmented using the deflection-bridging algorithm, as in (*35*). For RNA FISH measurements, cells were segmented for their whole-cell regions by spatially approximating an area encompassing the nucleus and reaching as far as 15 mm outside of the nuclear mask without overlapping other cell regions. This region will hereafter be referred to as the “whole-cell region”. RNA FISH puncta were segmented by top-hat filtering of the raw image with a circular kernel of radius 1.3 μm and thresholding on a constant background value determined against no probe control sample. The RNA puncta count for a given cell was calculated as the number of foreground pixels within that cell’s whole-cell region. Each whole-cell region was label-matched with its associated nucleus to enable single-cell comparisons of RNA puncta count with a given nuclear marker of interest. In the case of normal smFISH, all cell nucleus were stained with DAPI for segmentation. In the case of experiments testing the effect of CARGO labeling on the transcription output (fig. S4), cells were classified by the presence/absence of tagBFP, which is encoded by CARGO plasmid as an indicator of positive transfection.

Gu et al., 2017. figure S1

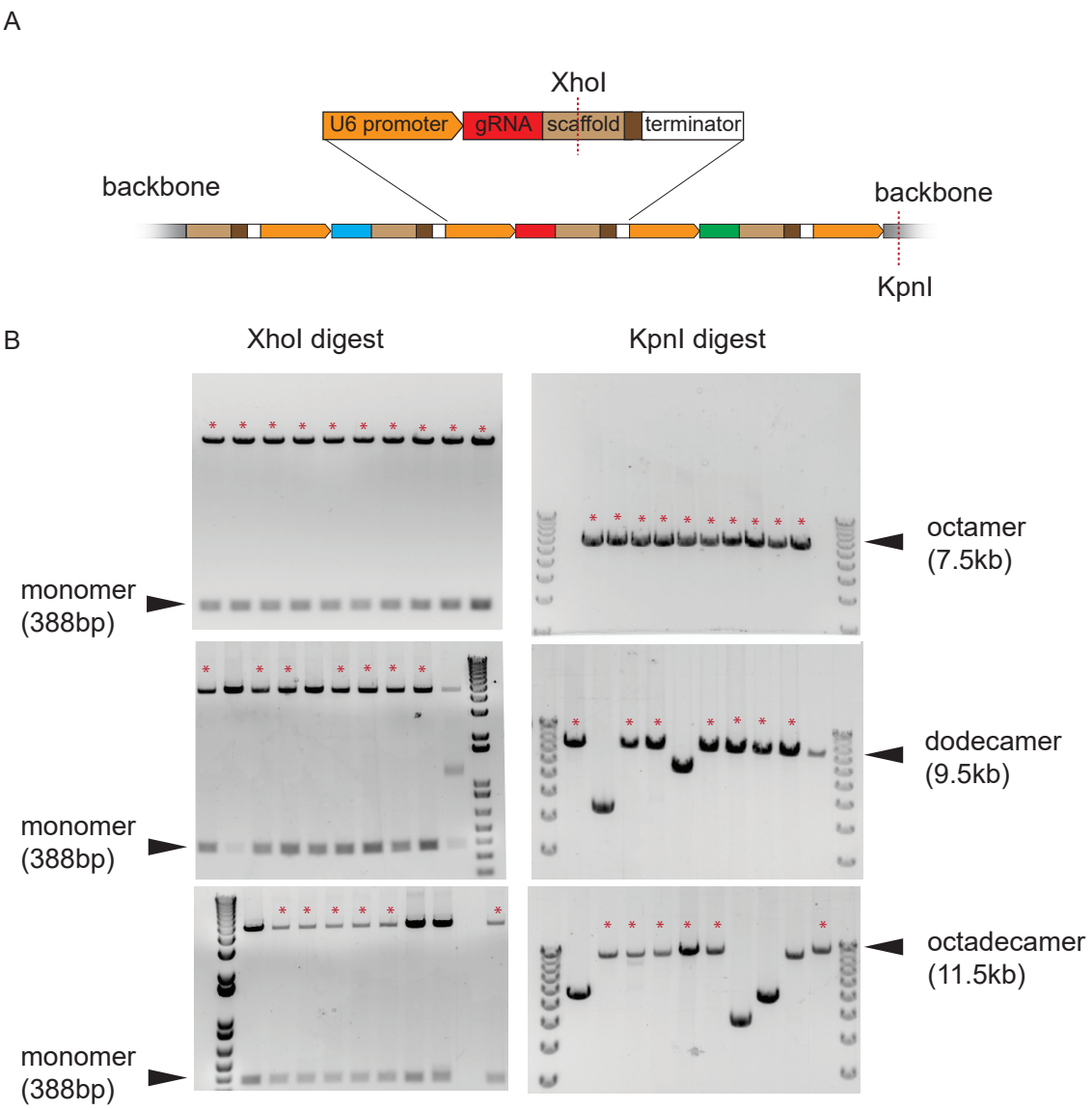


**fig. S1. Validation and efficiency of CARGO assembly. A.** Schematic view of a CARGO array with one repeat unit magnified, and indication of restriction sites for XhoI, which cuts within repeat unit, and KpnI, which cuts within plasma backbone outside of the array. **B.** Restriction digest of purified plasmids to test the size of assembled product. Red stars indicate correct products. Arrow indicates size corresponding to the size of expected correct product.

Gu et al., 2017. figure S2

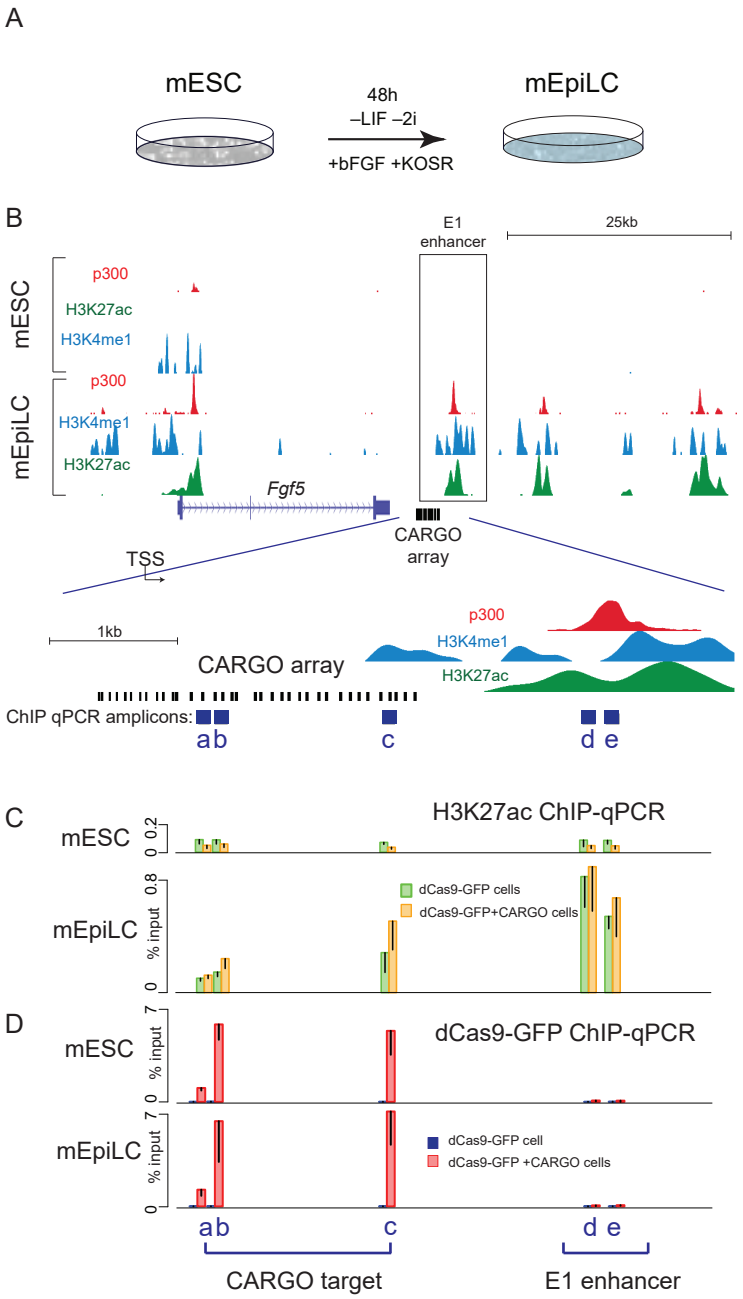


**fig. S2. Validation of the specificity and non-invasiveness of CARGO-dCas9 labeling. A.** Schematic representation of the transition between mESC and mEpiLC (see methods for detail). **B**. Schematic of the *Fgf5* locus with genome-browser tracks of ChIP-seq signals of active enhancer marks including p300, H3K27ac and H3K4me1 during mESC to mEpiLC transition. Positions of the designed CARGO array gRNAs are indicated by thin black bars below the browser tracks of active enhancer marks. Transcription start site and transcription directionality is denoted by TSS and angle arrow, respectively. The region of first enhancer (E1) of the *Fgf5* enhancer cluster is outlined by rectangle and a zoomed-in view of E1 region is provided at the bottom. ChIP-qPCR amplicons are indicated by solid dark blue squares denoted as a-e below the ChIP-seq tracks. **C.** Presence of CARGO-dCas9 does not interfere with enhancer activation during mESC-mEpiLC transition. H3K27ac ChIP-qPCR results from dCas9-eGFP cells with (orange bars) or without (green bars) *Fgf5* enhancer CARGO arrays are shown for regions corresponding to amplicons spanning CARGO targeted region (a-c) and *Fgf5* E1 enhancer (d and e). Fraction of ChIP DNA recovered relative to input is plotted, error bars correspond to standard deviation of the sample. **D.** dCas9 binds its target region in a CARGO-dependent manner, but does not spread to nearby enhancer. dCas9 ChIP-qPCR from dCas9-eGFP cells with (red bars) or without (blue bars) Fgf5 enhancer CARGO arrays are shown for regions corresponding to amplicons described in (H). Fraction of ChIP DNA recovered relative to input is plotted, error bars correspond to standard deviation of the sample.

Gu et al., 2017. figure S3

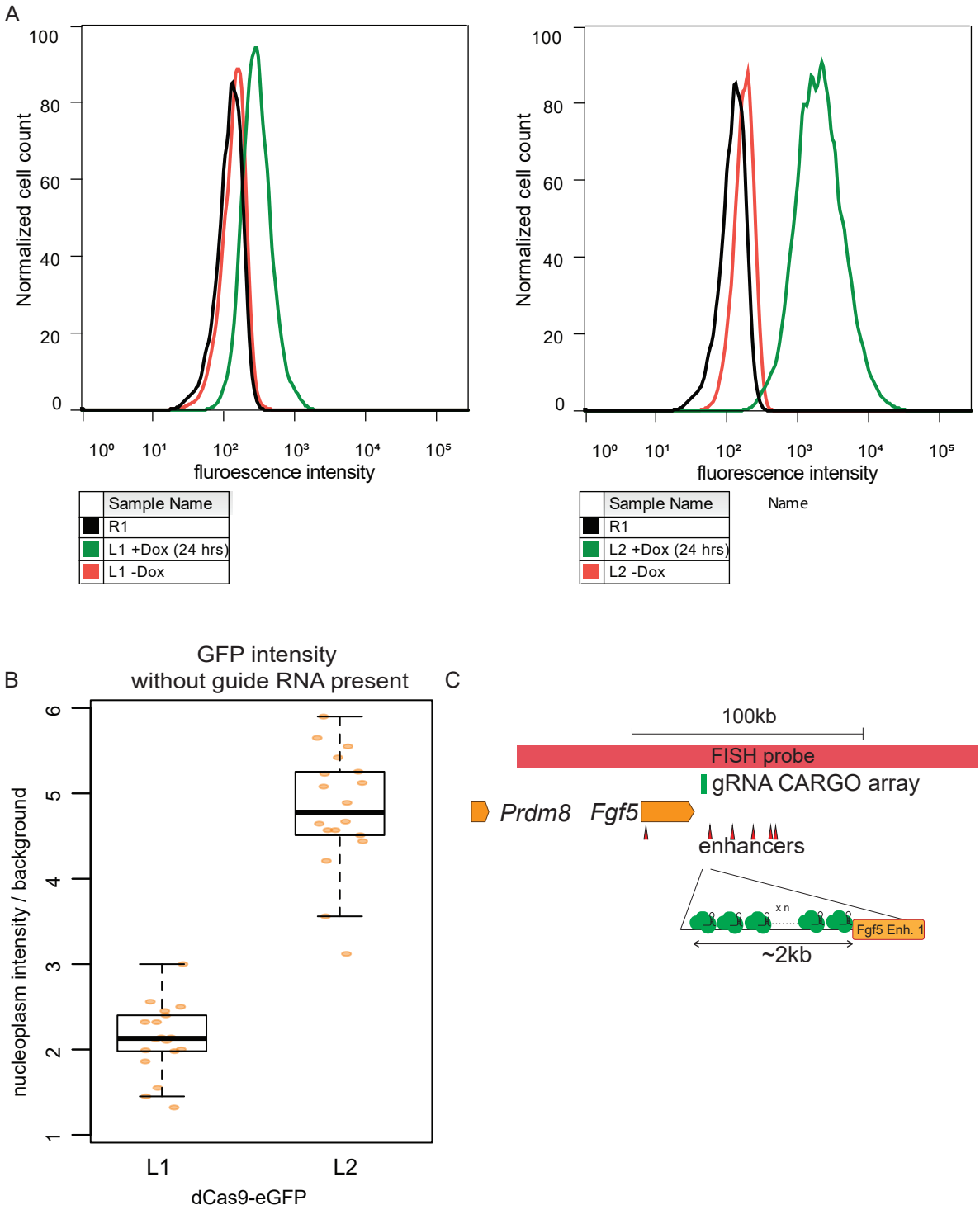


**fig. S3. Characterization of cell lines for CARGO-dCas9 imaging. A**. FACS analysis of induction of the dCas9-GFP expression in clonal mESC L1 and L2 lines. mESC cell lines with stably integrated dCas9-eGFP were treated with Doxycycline (Dox) for 24 hrs to induce dCas9-eGFP expression. Plotted are histograms of GFP fluorescence distribution in FACS analyze for wild-type parental mESC line—black line, dCas9-GFP lines without induction—red lines and dCas9-GFP lines with induction—green lines. Left panel Line 1 (L1), right panel Line 2 (L2) **B.** Box plot showing microscopic quantification of dCas9-GFP nucleoplasm fluorescence for 2 clonal mESC lines stably integrated with dCas9-GFP construct upon 24 hrs of Dox treatment. (n > 20 for all lines) **C.** Schematic of *Fgf5* locus with position of enhancers indicated as red arrowheads pointing upwards, genes as horizontal orange arrows, target of gRNA array as a green rectangle and *Fgf5* locus FISH probe as a red rectangle.

Gu et al., 2017. figure S4

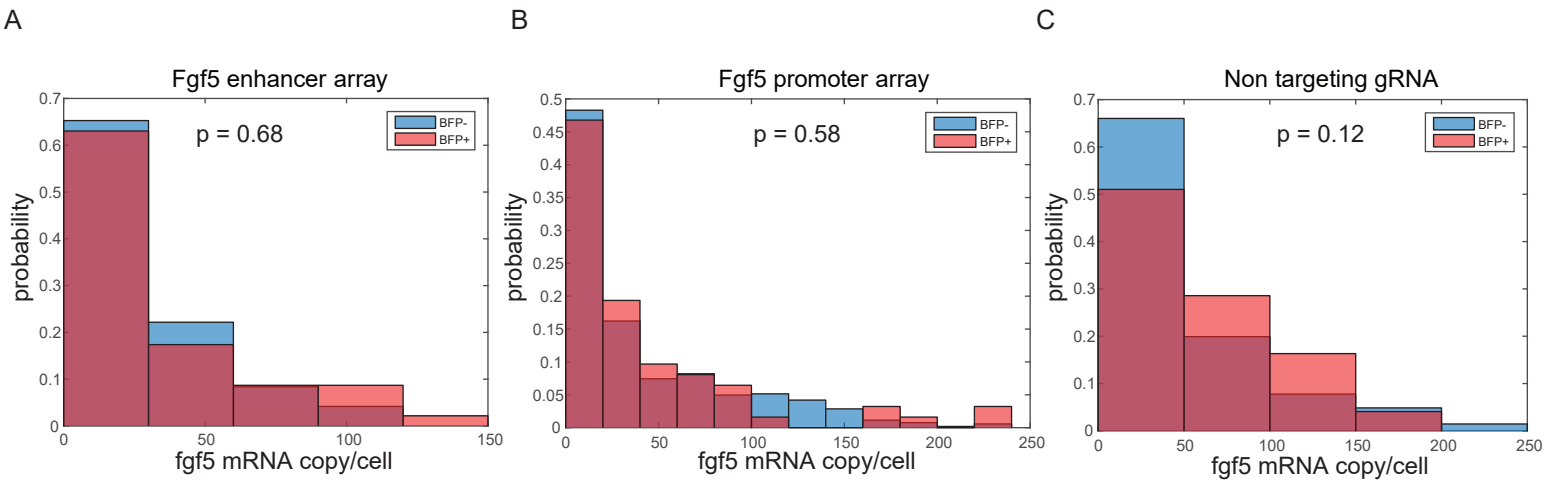


**fig. S4. Labeling of the *Fgf5* enhancer or promoter by CARGO does not interfere with *Fgf5* mRNA production.** Histograms of distribution of *Fgf5* mRNA copies per cell in EpiLC population of dCas9-GFP cells either non-transfected with CARGO array (blue bars) or successfully transfected with indicated CARGO array (red bars), as measured by smFISH. No significant differences between the transfected and non-transfected cells were detected by exact Wilcoxon-Mann-Whitney test. **A.** Fgf5 enhancer array (positive n=46, negative n=241), **B.** *Fgf5* promoter array (positive n=62, negative n=524), **C.** non-targeting array (positive n=49, negative n=206).

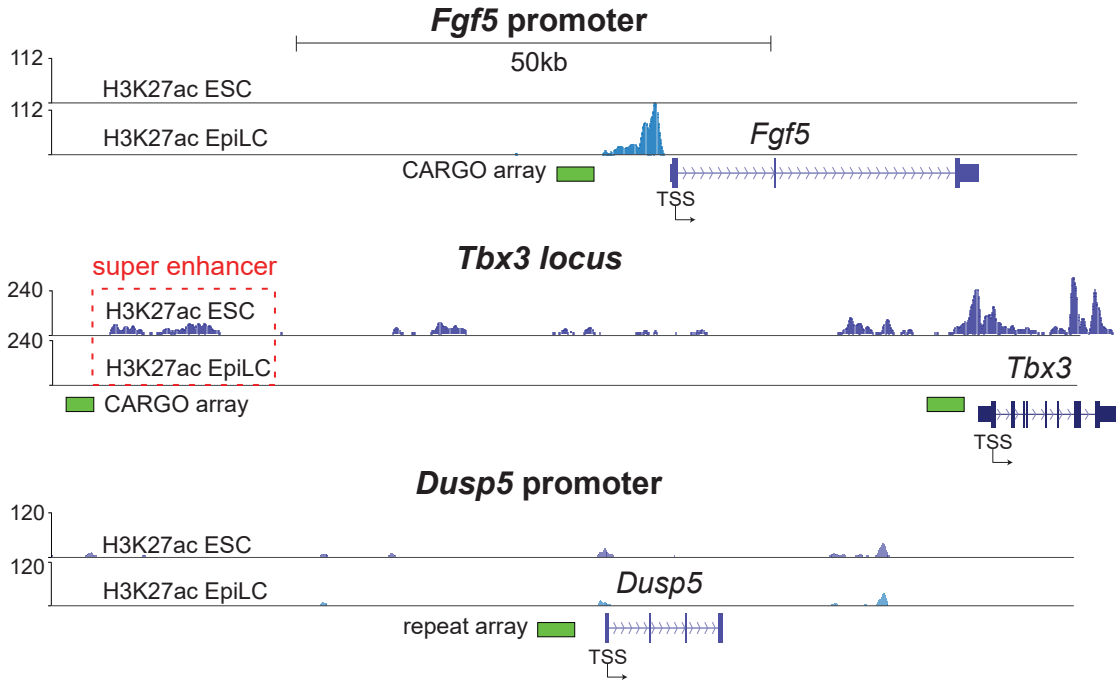


**fig. S5. Genome browser tracks of H3K27ac ChIP-seq at *Fgf5*, *Tbx3* and *Dusp5* loci in mESC and mEpiLC.** Positions of CARGO array (upstream of *Fgf5* promoter, *Tbx3* promoters and *Tbx3* super-enhancers) or local repeat (upstream of the *Dusp5* promoter) are indicated with solid green box. Transcription start site and transcription directionality is denoted by TSS and angle arrow, respectively.

Gu et al., 2017. figure S6

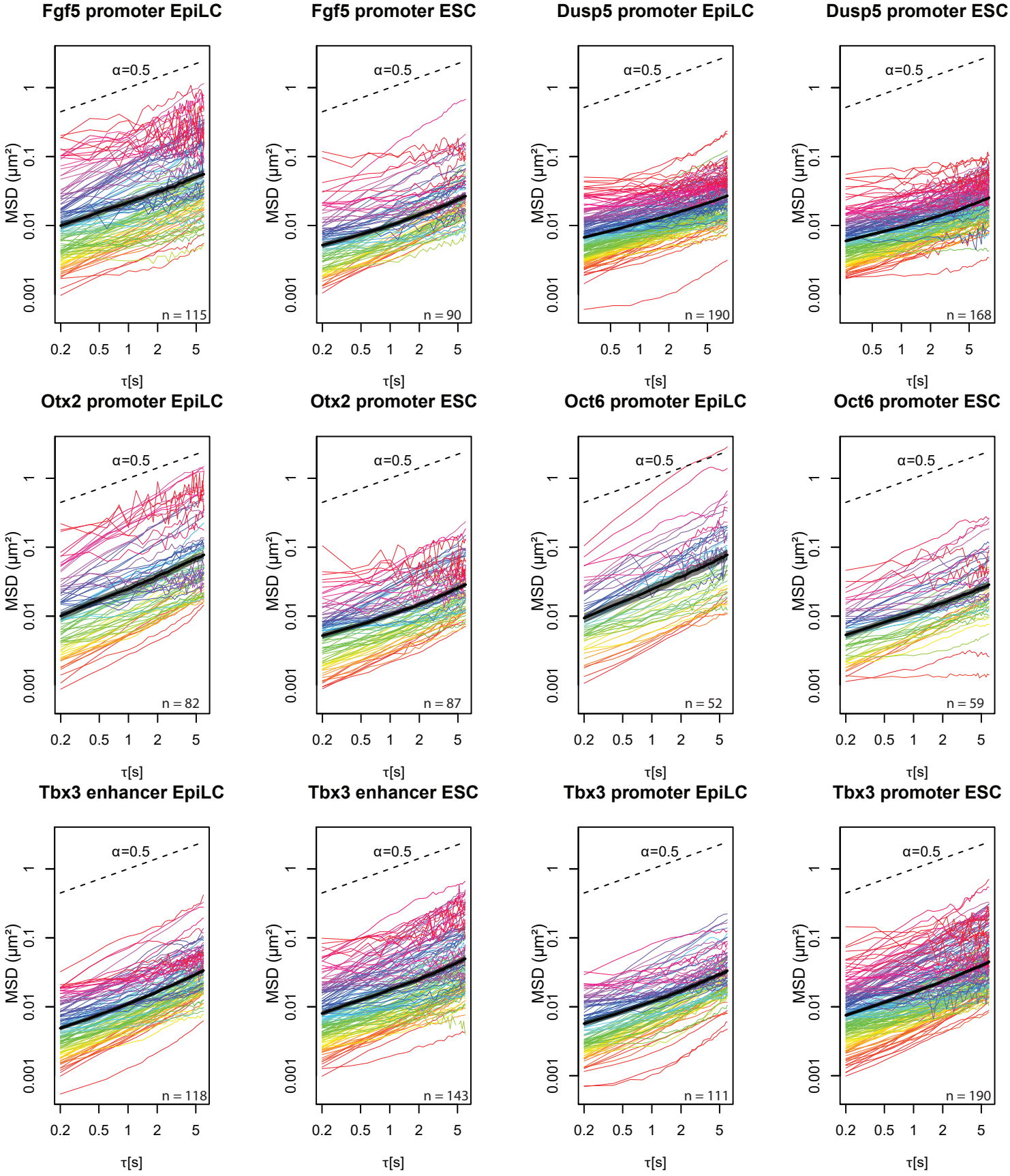


**fig. S6. MSD analyses for all tested cis-regulatory elements.** Time-averaged mean square displacements (colored curves) and time- and ensemble-averaged mean square displacements (black bold curve with shaded area showing ± s.e.m.) for each tracked loci (colored curves) as a function of time interval (τ) between observations. Loci names and cell states are denoted at the top of each panel. Number of observations are denoted at lower right corner of each panel. Black dashed lines: scaling guide with slope = 0.5.

Gu et al., 2017. figure S7

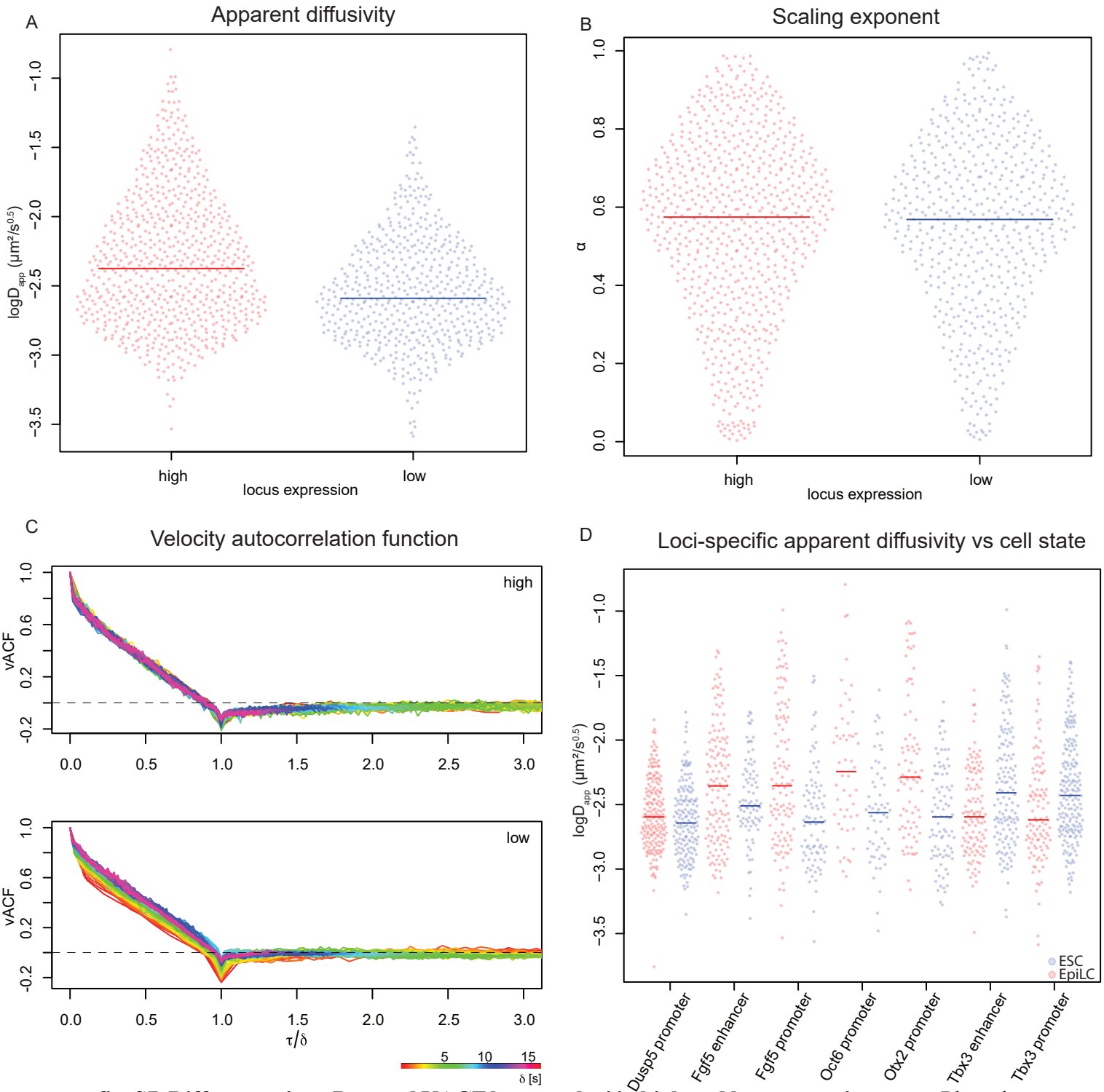


**fig. S7. Differences in α, $D_{app}$ and VACF between loci in high and low expression state.** Plotted as 1D scatterplots are combined fitted values for loci classified as being inferred high expression (e.g. *Tbx3* in mESC, *Fgf5* in mEpiLC) and low expression (e.g. *Tbx3* in mEpiLC, *Fgf5* in mESC) based on RNAseq data. Each dot corresponds to independent tracked locus, horizontal lines represent medians. **A.** Significantly larger apparent diffusion coefficient is observed for loci in higher expression states, $p<7.5\times10^{-16}$, Wilcoxon test. Dusp5 was excluded from the analysis due to significantly different image acquisition modality. **B.** no significant changes in scaling component are detected, p=0.75, Wilcoxon test. **C.** The sub-diffusion mechanism does not change significantly between low and high expression states, as evidenced by comparable shape and negative correlation peaks for velocity autocorrelation function (VACF) between high and low expression states. **D.** loci-specific apparent diffusion coefficient correlates with expression state. Plotted as 1D scatterplots are fitted $\log_{10}D_{app}$ from tMSD measurement of each labeled cis-regulatory element in either ESC (blue) or EpiLC (red) state. Horizontal lines indicate median.

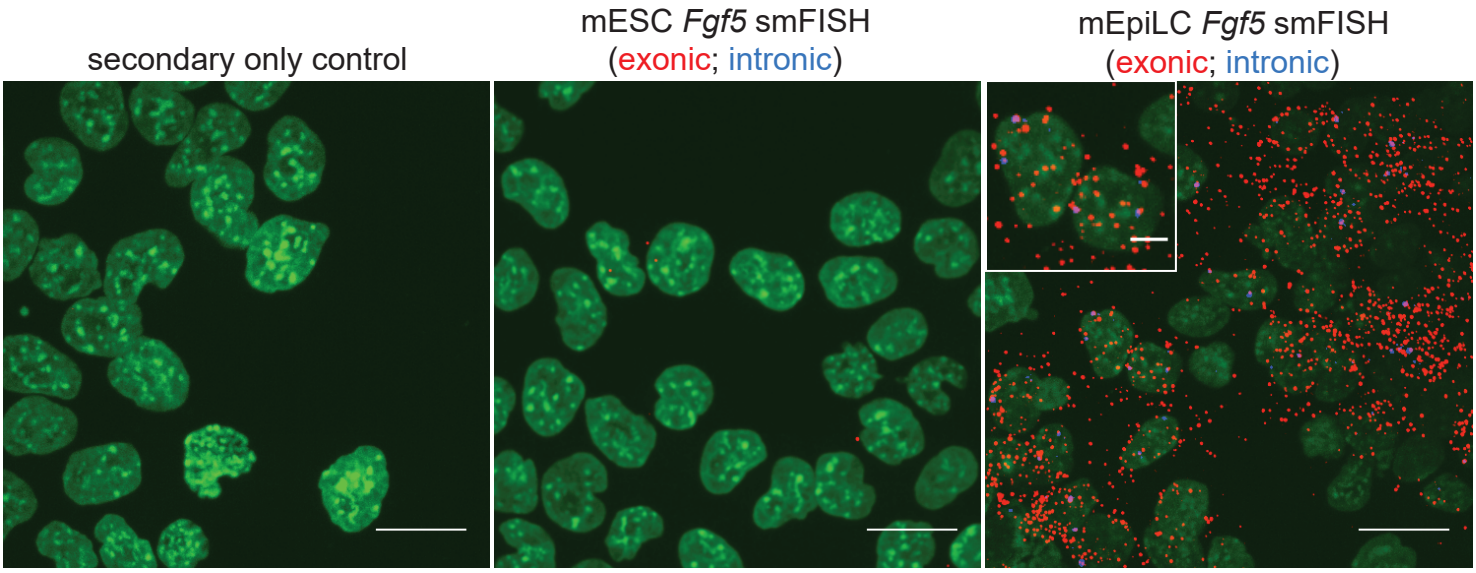


**fig. S8. Specificity validation of multiplexed smFISH.** Representative images showing specific colocalized *Fgf5* exonic-intronic smFISH signal. All smFISH experiments were done following a modified protocol from Affymetrix. Leftmost panel: smFISH with preamplifier and amplifier only middle panel: smFISH with Fgf5 intronic and exonic probes in mESC state; smFISH with *Fgf5* intronic and exonic probes in mEpiLC state. scalebar: 20 μm. Inset within rightmost panel: a magnified view of two individual cells with colocalized *Fgf5* exonic/intronic signal. Scalebar: 5 μm. Green: DAPI channel; red: *Fgf5* exonic channel; blue: *Fgf5* intronic channel. To quantify the labeling specificity, pixels from intronic and exonic channels were sparsely sampled (every 10th row and column) to avoid non-independent measurements and binarized by either above or below the detection threshold for intronic and exonic smFISH signals. Colocalization is confirmed by Fisher's exact test: $p < 2.12 \times 10^{-31}$, odds ratio 101.8 of non-random association between the binarized pixels.

Gu et al., 2017. figure S9

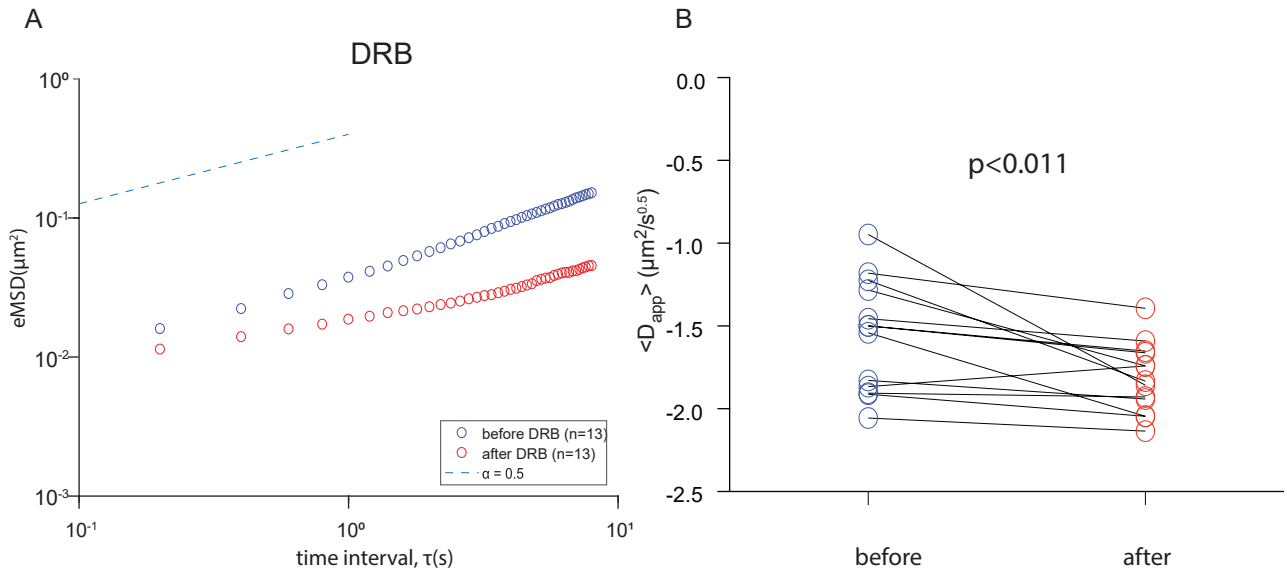


**fig. S9. Transcription inhibition reduces the diffusivity of the *Tbx3* promoter in mESCs. A.** time- and ensemble-averaged MSD (eMSD) plot for the *Tbx3* promoter in mESC state in non-drug treated (blue hollow circle) and DRB treated condition (red hollow circle) **B.** Anomalous diffusion coefficient extracted from time-averaged MSD of *Tbx3* promoter trajectories of the same cells before and after DRB treatment (same dataset as panel A). The decrease in diffusivity is supported by paired Wilcoxon test ($p<0.011$).

Table S1: BIC values for Gaussian mixture fits

| Locus: | Element: | Cell state: | number of fitted components: 1 | 2 | 3 |
|---|---|---|---|---|---|
| Dusp5 | promoter | mEpiLC | 68 .2 | 80.7 | NA |
| | | mESC | 63 .1 | 73.4 | 85.8 |
| Fgf5 | enhancer | mEpiLC | 183 .5 | 179.3 | 188.7 |
| | | mESC | 59 .0 | 65.5 | 73.5 |
| | promoter | mEpiLC | 197 .2 | 194.4 | 207.8 |
| | | mESC | 95 .9 | 101.2 | 112.7 |
| Oct6 | promoter | mEpiLC | 88 .6 | 96.3 | 102.0 |
| | | mESC | 63 .9 | 73.5 | 80.2 |
| Otx2 | promoter | mEpiLC | 140 .7 | 132.1 | 140.2 |
| | | mESC | 85 .1 | 91.3 | 104.2 |
| Tbx3 | enhancer | mEpiLC | 89 .5 | 97.3 | 99.3 |
| | | mESC | 194 .4 | 194.2 | 210.4 |
| | promoter | mEpiLC | 135 .2 | 136.3 | 149.1 |
| | | mESC | 193 .9 | 194.0 | 206.9 |

Table S2: Fitted values for dissusion parameters

| Locus: | Element: | Cell state: | n | $D_{app}$ [$\mu m^2 s^{-0.5}$] slow population | fast population | α |
|---|---|---|---|---|---|---|
| Dusp5 | promoter | mEpiLC | 190 | $2.9 \times 10^{-3 \pm 0.28}$ | | $0.43 \pm 0.17$ |
| | | mESC | 168 | $2.6 \times 10^{-3 \pm 0.28}$ | | $0.45 \pm 0.19$ |
| Fgf5 | enhancer | mEpiLC | 138 | $1.6 \times 10^{-3 \pm 0.16}$ | $8.6 \times 10^{-3 \pm 0.38}$ | $0.51 \pm 0.26$ |
| | | mESC | 86 | $3.9 \times 10^{-3 \pm 0.32}$ | | $0.53 \pm 0.21$ |
| | promoter | mEpiLC | 115 | $3.9 \times 10^{-3 \pm 0.32}$ | $26 \times 10^{-3 \pm 0.28}$ | $0.52 \pm 0.24$ |
| | | mESC | 90 | $3.0 \times 10^{-3 \pm 0.39}$ | | $0.52 \pm 0.26$ |
| Oct6 | promoter | mEpiLC | 52 | $2.0 \times 10^{-3 \pm 0.21}$ | $12.5 \times 10^{-3 \pm 0.48}$ | $0.63 \pm 0.20$ |
| | | mESC | 59 | $3.3 \times 10^{-3 \pm 0.39}$ | | $0.51 \pm 0.21$ |
| Otx2 | promoter | mEpiLC | 82 | $4.5 \times 10^{-3 \pm 0.35}$ | $52 \times 10^{-3 \pm 0.17}$ | $0.61 \pm 0.22$ |
| | | mESC | 87 | $3.1 \times 10^{-3 \pm 0.37}$ | | $0.54 \pm 0.23$ |
| Tbx3 | enhancer | mEpiLC | 118 | $3.2 \times 10^{-3 \pm 0.34}$ | | $0.60 \pm 0.19$ |
| | | mESC | 143 | $1.9 \times 10^{-3 \pm 0.16}$ | $7.9 \times 10^{-3 \pm 0.45}$ | $0.55 \pm 0.21$ |
| | promoter | mEpiLC | 111 | $3.7 \times 10^{-3 \pm 0.43}$ | | $0.55 \pm 0.22$ |
| | | mESC | 190 | $2.6 \times 10^{-3 \pm 0.24}$ | $10.7 \times 10^{-3 \pm 0.30}$ | $0.54 \pm 0.23$ |

**Table S3 (separate file). Guide RNA sequences used for dCas9 imaging in this study.**

**Movie S1**

***Fgf5* enhancer CARGO-dCas9 labeling and sub-second tracking.** Representative time-lapse movie of a single mESC with two alleles of *Fgf5* enhancer (E1) labelled by CARGO-dCas9. Frame rate: 5Hz. Scale bar: 2 μm. Red (allele 1) and blue (allele 2) empty circles: centers of the circle denote the sub-pixel precision coordinates of tracked loci in each frame. Timestamp unit: s.

**Movie S2**

**Movement of the CARGO-dCas9 labeled *Fgf5* enhancer in mESC.** Representative time-lapse movie of a single mESC with two labeled *Fgf5* enhancer alleles. Frame rate: 5Hz. Scale bar: 2 μm. Red (allele 1) and blue (allele 2) empty circles: centers of the circle denote the sub-pixel precision coordinates of tracked loci in each frame. Timestamp unit: s.

**Movie S3**

**Movement of the CARGO-dCas9 labeled *Fgf5* enhancer in mEpiLC.** Representative time-lapse movie of a single mEpiLC with two labeled *Fgf5* enhancer alleles. Frame rate: 5Hz. Scale bar: 2 μm. Red (allele 1) and blue (allele 2) empty circles: centers of the circle denote the sub-pixel precision coordinates of tracked loci in each frame. Timestamp unit: s.

**Movie S4**

**Movement of the CARGO-dCas9 labeled *Tbx3* promoter in mESC.** Representative time-lapse movie of a single mESC with two alleles of *Tbx3* promoter labelled by CARGO-dCas9. Frame rate: 5Hz. Scale bar: 2 μm. Red (allele 1) and blue (allele 2) empty circles: centers of the circle denote the sub-pixel precision coordinates of tracked loci in each frame. Timestamp unit: s.

**Movie S5**

**Movement of the CARGO-dCas9 labeled *Tbx3* promoter in mEpiLC.** Representative time-lapse movie of a single mEpiLC with two alleles of *Tbx3* promoter labelled by CARGO-dCas9. Frame rate: 5Hz. Scale bar: 2 μm. Red (allele 1) and blue (allele 2) empty circles: centers of the circle denote the sub-pixel precision coordinates of tracked loci in each frame. Timestamp unit: s.

**Additional Supplemental Script (separate file)**

**Additional bench protocol for CARGO assembly (separate file)**

**References and Notes**


1. H. K. Long, S. L. Prescott, J. Wysocka, Ever-changing landscapes: Transcriptional enhancers in development and evolution. *Cell* **167**, 1170–1187 (2016). doi:10.1016/j.cell.2016.09.018 Medline

2. M. Levine, Transcriptional enhancers in animal development and evolution. *Curr. Biol.* **20**, R754–R763 (2010). doi:10.1016/j.cub.2010.06.070 Medline

3. J. Dekker, L. Mirny, The 3D genome as moderator of chromosomal communication. *Cell* **164**, 1110–1121 (2016). doi:10.1016/j.cell.2016.02.007 Medline

4. S. Remeseiro, A. Hörnblad, F. Spitz, Gene regulation during development in the light of topologically associating domains. *WIREs Dev. Biol.* **5**, 169–185 (2016). doi:10.1002/wdev.218 Medline

5. H. J. Nielsen, Y. Li, B. Youngren, F. G. Hansen, S. Austin, Progressive segregation of the *Escherichia coli* chromosome. *Mol. Microbiol.* **61**, 383–393 (2006). doi:10.1111/j.1365-2958.2006.05245.x Medline

6. C. C. Robinett, A. Straight, G. Li, C. Willhelm, G. Sudlow, A. Murray, A. S. Belmont, In vivo localization of DNA sequences and visualization of large-scale chromatin organization using lac operator/repressor recognition. *J. Cell Biol.* **135**, 1685–1700 (1996). doi:10.1083/jcb.135.6.1685 Medline

7. W. F. Marshall, A. Straight, J. F. Marko, J. Swedlow, A. Dernburg, A. Belmont, A. W. Murray, D. A. Agard, J. W. Sedat, Interphase chromosomes undergo constrained diffusional motion in living cells. *Curr. Biol.* **7**, 930–939 (1997). doi:10.1016/S0960-9822(06)00412-X Medline

8. J. S. Lucas, Y. Zhang, O. K. Dudko, C. Murre, 3D trajectories adopted by coding and regulatory DNA elements: First-passage times for genomic interactions. *Cell* **158**, 339–352 (2014). doi:10.1016/j.cell.2014.05.036 Medline

9. J. Vazquez, A. S. Belmont, J. W. Sedat, Multiple regimes of constrained chromosome motion are regulated in the interphase *Drosophila* nucleus. *Curr. Biol.* **11**, 1227–1239 (2001). doi:10.1016/S0960-9822(01)00390-6 Medline

10. S. H. Mitsuda, N. Shimizu, Epigenetic repeat-induced gene silencing in the chromosomal and extrachromosomal contexts in human cells. *PLOS ONE* **11**, e0161288 (2016). doi:10.1371/journal.pone.0161288 Medline

11. B. Chen, L. A. Gilbert, B. A. Cimini, J. Schnitzbauer, W. Zhang, G.-W. Li, J. Park, E. H. Blackburn, J. S. Weissman, L. S. Qi, B. Huang, Dynamic imaging of genomic loci in living human cells by an optimized CRISPR/Cas system. *Cell* **155**, 1479–1491 (2013). doi:10.1016/j.cell.2013.12.001 Medline

12. B. Chen, J. Hu, R. Almeida, H. Liu, S. Balakrishnan, C. Covill-Cooke, W. A. Lim, B. Huang, Expanding the CRISPR imaging toolset with *Staphylococcus aureus* Cas9 for simultaneous imaging of multiple genomic loci. *Nucleic Acids Res.* **44**, e75 (2016). Medline

13. H. Ma, A. Naseri, P. Reyes-Gutierrez, S. A. Wolfe, S. Zhang, T. Pederson, Multicolor CRISPR labeling of chromosomal loci in human cells. *Proc. Natl. Acad. Sci. U.S.A.* **112**, 3002–3007 (2015). doi:10.1073/pnas.1420024112 Medline

14. H. Ma, L.-C. Tu, A. Naseri, M. Huisman, S. Zhang, D. Grunwald, T. Pederson, Multiplexed labeling of genomic loci with dCas9 and engineered sgRNAs using CRISPRainbow. *Nat. Biotechnol.* **34**, 528–530 (2016). doi:10.1038/nbt.3526 Medline

15. Y. Fu, P. P. Rocha, V. M. Luo, R. Raviram, Y. Deng, E. O. Mazzoni, J. A. Skok, CRISPR-dCas9 and sgRNA scaffolds enable dual-colour live imaging of satellite sequences and repeat-enriched individual loci. *Nat. Commun.* **7**, 11707 (2016). Medline

16. K. Hayashi, H. Ohta, K. Kurimoto, S. Aramaki, M. Saitou, Reconstitution of the mouse germ cell specification pathway in culture by pluripotent stem cells. *Cell* **146**, 519–532 (2011). doi:10.1016/j.cell.2011.06.052 Medline

17. C. Buecker, R. Srinivasan, Z. Wu, E. Calo, D. Acampora, T. Faial, A. Simeone, M. Tan, T. Swigut, J. Wysocka, Reorganization of enhancer patterns in transition from naive to primed pluripotency. *Cell Stem Cell* **14**, 838–853 (2014). doi:10.1016/j.stem.2014.04.003 Medline

18. T. Kalkan, A. Smith, Mapping the route from naive pluripotency to lineage specification. *Philos. Trans. R. Soc. London Ser. B* **369**, 20130540 (2014). doi:10.1098/rstb.2013.0540 Medline

19. S. C. Weber, A. J. Spakowitz, J. A. Theriot, Bacterial chromosomal loci move subdiffusively through a viscoelastic cytoplasm. *Phys. Rev. Lett.* **104**, 238102 (2010). doi:10.1103/PhysRevLett.104.238102 Medline

20. G. G. Cabal, A. Genovesio, S. Rodriguez-Navarro, C. Zimmer, O. Gadal, A. Lesne, H. Buc, F. Feuerbach-Fournier, J.-C. Olivo-Marin, E. C. Hurt, U. Nehrbass, SAGA interacting factors confine sub-diffusion of transcribed genes to the nuclear envelope. *Nature* **441**, 770–773 (2006). doi:10.1038/nature04752 Medline

21. S.-H. Chao, K. Fujinaga, J. E. Marion, R. Taube, E. A. Sausville, A. M. Senderowicz, B. M. Peterlin, D. H. Price, Flavopiridol inhibits P-TEFb and blocks HIV-1 replication. *J. Biol. Chem.* **275**, 28345–28348 (2000). doi:10.1074/jbc.C000446200 Medline

22. K. Yankulov, K. Yamashita, R. Roy, J.-M. Egly, D. L. Bentley, The transcriptional elongation inhibitor 5,6-dichloro-1-β-D-ribofuranosylbenzimidazole inhibits transcription factor IIH-associated protein kinase. *J. Biol. Chem.* **270**, 23922–23925 (1995). doi:10.1074/jbc.270.41.23922 Medline

23. D. V. Titov, B. Gilman, Q.-L. He, S. Bhat, W.-K. Low, Y. Dang, M. Smeaton, A. L. Demain, P. S. Miller, J. F. Kugel, J. A. Goodrich, J. O. Liu, XPB, a subunit of TFIIH, is a target of the natural product triptolide. *Nat. Chem. Biol.* **7**, 182–188 (2011). doi:10.1038/nchembio.522 Medline

24. S. Vispé, L. DeVries, L. Créancier, J. Besse, S. Bréand, D. J. Hobson, J. Q. Svejstrup, J.-P. Annereau, D. Cussac, C. Dumontet, N. Guilbaud, J.-M. Barret, C. Bailly, Triptolide is an inhibitor of RNA polymerase I and II-dependent transcription leading predominantly to down-regulation of short-lived mRNA. *Mol. Cancer Ther.* **8**, 2780–2790 (2009). doi:10.1158/1535-7163.MCT-09-0549 Medline

25. Y. Zhang, O. K. Dudko, First-passage processes in the genome. *Annu. Rev. Biophys.* **45**, 117–134 (2016). doi:10.1146/annurev-biophys-062215-010925 Medline

26. S. C. Weber, A. J. Spakowitz, J. A. Theriot, Nonthermal ATP-dependent fluctuations contribute to the in vivo motion of chromosomal loci. *Proc. Natl. Acad. Sci. U.S.A.* **109**, 7338–7343 (2012). doi:10.1073/pnas.1119505109 Medline

27. T. Cermak, E. L. Doyle, M. Christian, L. Wang, Y. Zhang, C. Schmidt, J. A. Baller, N. V. Somia, A. J. Bogdanove, D. F. Voytas, Efficient design and assembly of custom TALEN and other TAL effector-based constructs for DNA targeting. *Nucleic Acids Res.* **39**, e82 (2011). doi:10.1093/nar/gkr218 Medline

28. D. S. Martin, M. B. Forstner, J. A. Käs, Apparent subdiffusion inherent to single particle tracking. *Biophys. J.* **83**, 2109–2117 (2002). doi:10.1016/S0006-3495(02)73971-4 Medline

29. M. O. Prates, V. H. Lachos, C. R. B. Cabral, mixsmsn: Fitting finite mixture of scale mixture of skew-normal distributions. *J. Stat. Softw.* **54**, 1–20 (2013). doi:10.18637/jss.v054.i12

30. G. E. Box, G. M. Jenkins, G. C. Reinsel, G. M. Ljung, *Time Series Analysis: Forecasting and Control* (John Wiley & Sons, 2015).

31. X. Ji, Y. Zhou, S. Pandit, J. Huang, H. Li, C. Y. Lin, R. Xiao, C. B. Burge, X.-D. Fu, SR proteins collaborate with 7SK and promoter-associated nascent RNA to release paused polymerase. *Cell* **153**, 855–868 (2013). doi:10.1016/j.cell.2013.04.028 Medline

32. A. Rada-Iglesias, R. Bajpai, T. Swigut, S. A. Brugmann, R. A. Flynn, J. Wysocka, A unique chromatin signature uncovers early developmental enhancers in humans. *Nature* **470**, 279–283 (2011). doi:10.1038/nature09692 Medline

33. J. Chaumeil, S. Augui, J. C. Chow, E. Heard, "Combined immunofluorescence, RNA fluorescent in situ hybridization, and DNA fluorescent in situ hybridization to study chromatin changes, transcriptional activity, nuclear organization, and X-chromosome inactivation." *The Nucleus: Volume 1: Nuclei and Subnuclear Components*, 297–308 (2008).

34. U. Moran, R. Phillips, R. Milo, SnapShot: Key numbers in biology. *Cell* **141**, 1262–1262.e1 (2010). doi:10.1016/j.cell.2010.06.019 Medline

35. S. D. Cappell, M. Chung, A. Jaimovich, S. L. Spencer, T. Meyer, Irreversible $APC^{Cdh1}$ inactivation underlies the point of no return for cell-cycle entry. *Cell* **166**, 167–180 (2016). doi:10.1016/j.cell.2016.05.077 Medline